# ULTRASOUND ASSISTED BISMUTH COATED IRON OXIDE NANOPARTICLES FOR A POTENTIAL DUAL-MODAL CT/MR IMAGING CONTRAST MEDIA

**FARHANK SABER BRAIM**

**UNIVERSITI SAINS MALAYSIA**

**2024**

# ULTRASOUND ASSISTED BISMUTH COATED IRON OXIDE NANOPARTICLES FOR A POTENTIAL DUAL-MODAL CT/MR IMAGING CONTRAST MEDIA

**by**

**FARHANK SABER BRAIM**

**Thesis submitted in fulfilment of the requirements**
**for the degree of**
**Doctor of Philosophy**

**February 2024**

## ACKNOWLEDGEMENT

First and foremost, I would like to deeply thank the Almighty Allah for granting me the good health that was necessary to complete this journey and the strength and patience to achieve my goals.

Next, I would like to express my sincere appreciation to my supervisor, Dr. Nik Noor Ashikin Nik Abd Razak for her endless support, guidance, and kind cooperation throughout the research. Her great personality, being very considerate, and wisely solving problems have improved the quality of this dissertation. A very special gratitude goes to my co-supervisor Professor Dr. Azlan Abdul Aziz, for his support, constructive comments and suggestions, useful contribution, and valuable guidance.

I express appreciation to the staff of the Nano-Optoelectronics Research and Technology Laboratory (NOR lab) and Institute for Research in Molecular Medicine (INFORMM) lab assistants for technical assistance during my laboratory work, particularly in the sample characterizations.

I would like to express my profound gratitude to my family, especially my parents and my siblings for their continuous prayers and support. My deepest appreciation extends to my family members, my beloved wife Layla Qasim Ismael for her boundless support and encouragement, and my sons (Rawa and Rahand) for their patience and understanding. I could not have finished this journey without their love, affection, and concern. Finally, I thank all who supported me in any respect during the completion of this study.

## TABLE OF CONTENTS

## LIST OF TABLES

**Page**

## LIST OF FIGURES

**Page**

# LIST OF SYMBOLS

| | |
|---|---|
| °C | Degree Celsius |
| Oe | Oersted (magnetizing field) |
| Hz | Hertz |
| cm | Centimeter |
| nm | Nanometer |
| $B_o$ | Magnetic field |
| $\omega_o$ | Larmor frequency |
| $\gamma$ | Gyration ratio |
| HU | Hounsfield Units |
| $\mu$ | Attenuation coefficient |
| $\mu$l | Microliter |
| $\mu$g | Microgram |
| $d$ | Lattice spacing |
| $n$ | Integer number |
| $\lambda$ | Wavelength |
| $\theta$ | Angle |
| A° | Angstrom |
| $D$ | Crystallite size |
| K | Kelvin |
| atm | Atmosphere |
| $\zeta$ | Zeta potential |
| rpm | Revolution per minutes |
| $d_{hkl}$ | Interplanar spacing |
| h,k,l | Miller indices |

| | |
|---|---|
| a | Lattice constant |
| a.u. | Arbitrary unit |
| W | Watt |
| *W* | Weight |

## LIST OF ABBREVIATIONS

| | |
|---|---|
| Ag | Silver |
| ANOVA | Analysis of variance |
| Au | Gold |
| $BaSO_4$ | Barium sulfate |
| BBD | Behnken design |
| Bi | Bismuth |
| $Bi(NO_3)_3.5H_2O$ | Bismuth nitrate pentahydrate |
| $Bi_2O_3$ | Bismuth Oxide |
| $Bi^{3+}$ | Bismuth Ion/ Bismuth Cation |
| $BiFeO_3$ | Bismuth ferrite |
| $C_2H_5NO_2$ | Glycine |
| Cas | Contrast agents |
| CT scan | Computed Tomography scan |
| CVD | Chemical Vapor Deposition |
| DI | Deionized |
| DLS | Dynamic Light Scattering |
| DOE | Design of Experiments |
| EDX | Energy dispersive X-ray |
| EM | Electromagnetic |
| FBS | Fetal bovine serum |
| FCCD | Face-centered Center Composite Design |
| FCM | Flow cytometry |
| Fe | Iron |
| $Fe(NO_3)_3$ | Ferric nitrate |
| $Fe^{2+}$ | Ferrous ion |
| $Fe^{3+}$ | Ferric ion |
| $Fe_3O_4$ | Magnetite |
| $FeCl_2$ | Ferrous chloride |
| $FeCl_3$ | Ferric chloride |
| FeO | Wustite |
| FESEM | Field Emission Scanning Electron Microscopy |

| | |
|---|---|
| FS | Forwarded-scattered light |
| FTIR | Fourier Transform Infrared Spectroscopy |
| FWHM | Full-width half maximum |
| *Hc* | Coercive force |
| HPLC | High Performance Liquid Chromatography |
| I | Iodine |
| IC-PMS | Inductively Coupled Plasma Mass Spectrometer |
| IONPs | Iron Oxide Nanoparticles |
| IR | Infrared |
| $K_4Fe(CN)_6.3H_2O$ | Potassium hexacyanoferrate (II) trihydrate |
| KOH | Potassium hydroxide |
| *Mr* | Remanent magnetization |
| MRI | Magnetic Resonance Imaging |
| *Ms* | Saturation magnetization |
| $Na_2CO_3$ | Sodium carbonate |
| NaOH | Sodium hydroxide |
| $NH_4OH$ | Ammonium hydroxide |
| NIR | Near-infrared |
| NPs | Nanoparticles |
| OD | Optical density |
| PBS | Phosphate Buffer Saline |
| Pd | Palladium |
| PDI | Polydispersity index |
| PI | Propidium iodide |
| Pt | Platinum |
| PVD | Physical Vapor Deposition |
| $r_2$ | Longitudinal Relaxation rate |
| RES | Reticuloendothelial systems |
| RF | Radio frequency |
| RSM | Response surface methodology |
| SBH, $NaBH_4$ | Sodium borohydride |
| SCW | Supercritical water |
| SPIONs | Superparamagnetic iron oxide nanoparticles |
| SPR | Surface plasmon resonance |

| | |
|---|---|
| SS | Side-scattered light |
| $T_1$ | Longitudinal Relaxation Time |
| $T_2$ | Transverse Relaxation Time |
| TE | Echo time |
| TEM | Transmission Electron Microscope |
| TR | Repetition Time |
| VSM | Vibrating Sample Magnetometer |
| Z | Atomic number |
| $\alpha$-$Fe_2O_3$ | Hematite |
| $\alpha$-FeOOH | Goethite |
| $\gamma$-$Fe_2O_3$ | Maghemite |

## LIST OF APPENDICES

**NANOPARTIKEL BESI OKSIDA BERSADUR BISMUT BERBANTUKAN ULTRASONIK YANG BERPOTENSI SEBAGAI MEDIA KONTRAS PENGIMEJAN DWI-MODAL CT/MR**

## ABSTRAK

Penggabungan zarah nano bismut (Bi NPs) dan zarah nano magnetit ($Fe_3O_4$ NPs) ke dalam nano kuar uji ($Fe_3O_4$@Bi) adalah teknik yang berpotensi tinggi berdasarkan sifat pengubahsuaian, penstabilan dan pelbagai fungsinya dalam aplikasi bioperubatan. Walau bagaimanapun, kaedah konvensional untuk menghasilkan NP komposit Bi/$Fe_3O_4$ adalah memerihkan, mengambil masa yang panjang, rumit dan mahal kerana memerlukan pelbagai jenis reagen. Dalam kajian ini, pengubahsuaian $Fe_3O_4$ NP secara pantas dapat dilakukan dengan menggunakan ultrasound melalui pensaduran permukaannya dengan Bi NP bagi menghasilkan NP komposit $Fe_3O_4$@Bi yang unik sebagai kegunaan imbasan tomografi (CT) dan pengimejan resonans magnetik (MRI). Pada mulanya, NP $Fe_3O_4$ dihasilkan melalui kaedah pemendakan bersama bantuan proses hijau. Selepas itu, NP komposit $Fe_3O_4$@Bi disintesis dan dioptimumkan secara statistik menggunakan kaedah sonokimia dan metodologi permukaan tindak balas (RSM). Reka bentuk komposit pemprosesan berpusat-muka (FCCD) mengkaji kesan tetapan penghasilan terhadap kestabilan, saiz dan taburan saiz nanokomposit. Parameter penghasilan yang dioptimumkan yang mempengaruhi tindak balas, masing-masing adalah 40 ml, 5 ml dan 12 min untuk kepekatan Bi, kepekatan natrium borohidrida (SBH), dan masa sonikasi. Nilai yang diramalkan untuk potensi zeta, saiz hidrodinamik, dan indeks polidispersiti (PdI) pada larutan kebolehinginan tertinggi (100%) ialah -45 mV, 172 nm, dan 0.257, manakala nilai eksperimen yang disahkan masing-masing ialah -47.1 mV, 125 nm, dan 0.281. Adalah

didapati bahawa masa sonikasi adalah faktor yang paling berpengaruh dalam semua respons. Sifat fizikokimia NP yang disintesis telah dicirikan menggunakan DLS, XRD, TEM, FESEM, EDX, RAMAN, FTIR, UV-visible, dan VSM. Berdasarkan analisis DLS, ultrasound menstabilkan dan memfungsikan $Fe_3O_4$ NP dengan ketara berikutan pengubahsuaiannya kepada $Fe_3O_4$@Bi NPs dan meningkatkan nilai potensi zeta daripada -33.5 kepada -47.1 mV, dan saiz hidrodinamik meningkat daripada 98 nm kepada 125 nm. Keputusan menunjukkan bahawa $Fe_3O_4$ NPs sebelum dan selepas pengubahsuaian adalah sfera dan mono-dispersi dengan saiz zarah purata 11.7 nm dan 19.5 nm, manakala nilai magnetisasi tepu (Ms) masing-masing ialah 132.33 emu/g dan 92.192 emu/g. Sitotoksisiti dan kadar penyerapan selular $Fe_3O_4$@Bi NPs pada sel THLE-2 dan HEK-293 menunjukan ia tidak ketoksikan, bergantung kepada masa, dan internalisasi bergantung kepada dos. $Fe_3O_4$@Bi NPs kemudiannya diuji untuk agen kontras CT dan MRI. Nilai pengecilan sinar-X dan pengenduran melintang ($r_2$) yang diukur menunjukkan nilai masing-masing 399.11 HU dan 273.06 $mM^{-1}$ $s^{-1}$ iaitu lebih besar daripada nilai NPs komersial dan juga nilai NPs yang dihasilkan melalui kaedah konvensional. Hasil kerja ini membuktikan kemajuan yang besar dalam mensintesis $Fe_3O_4$@Bi NPs yang berkualiti tinggi, stabil dan biokompatibel melalui kaedah yang cepat dan mudah dalam masa 12 minit dan nanokomposit mempunyai potensi besar sebagai agen kontras dwi-modal untuk pengimejan CT dan MRI.

**ULTRASOUND ASSISTED BISMUTH COATED IRON OXIDE NANOPARTICLES FOR A POTENTIAL DUAL-MODAL CT/MR IMAGING CONTRAST MEDIA**

## ABSTRACT

The incorporation of bismuth nanoparticles (Bi NPs) and magnetite nanoparticles ($Fe_3O_4$ NPs) into a single ($Fe_3O_4$@Bi) nanoprobe is a promising technique for their properties modification, stabilization, and multi-functionalization in biomedical applications. However, conventional methods of producing Bi/$Fe_3O_4$ composite NPs are laborious, time-consuming, complicated, and costly by requiring multiple reagents. In this study, ultrasound rapidly modified $Fe_3O_4$ NPs by coating their surface with Bi NPs, creating unique $Fe_3O_4$@Bi composite NPs for computed tomography (CT) scan and magnetic resonance imaging (MRI). Initially, $Fe_3O_4$ NPs were produced through the green-assisted co-precipitation method. Subsequently, the $Fe_3O_4$@Bi composite NPs were synthesized and statistically optimized using the sonochemical method and response surface methodology (RSM). A face-centered central composite design (FCCD) investigated the effect of preparation settings on the stability, size, and size distribution of the nanocomposite. The optimized preparation parameters that influenced the responses were determined to be 40 ml, 5 ml, and (12 min, 40 W, and 40%) for Bi volume, sodium borohydride (SBH) volume, and (sonication time, power, frequency), respectively. The predicted values for the zeta potential, hydrodynamic size, and polydispersity index (PdI) at the highest desirability solution (100%) were -45 mV, 122 nm, and 0.257, while the validated experimental values were -47.1 mV, 125 nm, and 0.281, respectively. It was found that the sonication time was the most influential factor in all of the responses. Physicochemical

properties of the synthesized NPs were characterized using DLS, XRD, TEM, FESEM, EDX, RAMAN, FTIR, UV-visible, and VSM. Based on the DLS analysis, ultrasound significantly stabilized and functionalized $Fe_3O_4$ NPs following modification to $Fe_3O_4$@Bi NPs and improved the zeta potential value from -33.5 to -47.1 mV, and the hydrodynamic size increased from 98 nm to 125 nm. The results revealed that $Fe_3O_4$NPs before and after modification were spherical and mono-dispersed with average particle sizes of 11.7 nm and 19.5 nm, while their saturation magnetization (*Ms*) values were 132.33 emu/g and 92.192 emu/g, respectively. The cytotoxicity and cellular uptake of $Fe_3O_4$@Bi NPs on THLE-2 and HEK-293 cells revealed non-toxicity, time-dependent, and dose-dependent internalization. The $Fe_3O_4$@Bi NPs were then tested for CT and MRI contrast agents. The X-ray attenuation and transverse relaxivity ($r_2$) values were measured to be 399.11 HU and 273.06 $mM^{-1}$ $s^{-1}$ are greater than those of Bi/$Fe_3O_4$ NPs produced by conventional methods. The results demonstrate that this work has considerable progress in synthesizing high-quality, stable, and biocompatible $Fe_3O_4$@Bi NPs through a rapid and facile method within 12 minutes and the nanocomposites have great potential as dual-modal contrast agents for CT and MRI imaging.

# CHAPTER 1

# INTRODUCTION

## 1.1 Nanoscience and nanotechnology

The prefix "nano" originates from the Greek word for "dwarf" or "extremely small," and it represents a measurement that is one thousand millionth of a meter ($10^{-9}$ m) in size. Nanoscience and nanotechnology should be distinguished. Nanotechnology refers to the technological implementation of nanoscience, which is the interdisciplinary study of structures and molecules at nanometer scales between 1 and 100 nm. Nanotechnology allows nanoscale material observation, quantification, manipulation, assembly, regulation, and production. It is a promising 21st-century technology. Richard Feynman, a Nobel Prize-winning physicist from the United States, introduces the notion of nanotechnology in 1959. In 1974, after fifteen years, Japanese scientist Norio Taniguchi was the first to adopt and define the term "nanotechnology" as: “Nanotechnology mainly consists of the processing of separation, consolidation, and deformation of materials by one atom or one molecule” [1].

The development of a scanning tunneling microscope capable of visualizing individual atoms was the beginning of modern nanotechnology. It has been established in nanoscale science and technology that materials at the nanoscale have properties (such as mechanical, optical, chemical, electrical, etc.) that are significantly different from those of bulk materials. The improved performance properties of nanoparticles (NPs) over bulk materials in similar applications have been established. The production of nanocatalysts, a novel form of catalysts, is considered as an essential application of NPs [2]. As an example, bulk gold is known to be inert and unreactive as a catalyst, whereas gold NPs demonstrate extremely high catalytic reactivity in a range of gas-phase reactions, such as carbon monoxide and alcohol oxidation [3]. In another

example, the antifungal activity of bismuth oxide ($Bi_2O_3$) nanoneedles against *C. albicans* was four times higher than that of the $Bi_2O_3$ bulk powder [4]. In contrast to their non-magnetic bulk counterparts, gold (Au), platinum (Pt), and palladium (Pd) nanoscale materials embedded in polymer displayed magnetic moments [5,6].

Two factors can explain why NPs' physicochemical properties differ significantly from those of their bulk counterparts: (1) the surface effect of nanoscale materials, in which the fraction of atoms at the surface has fewer neighboring atoms than those in the bulk form, and (2) quantum effects that exhibit discontinuous behavior as a result of shells completion in systems with delocalized electrons [7]. These unique features of NPs have led to their widespread use in numerous fields, including electronics, energy, telecommunication, and biomedicine. Nanomaterials exploited in biomedical and related applications include polymeric micelles, liposomes, block ionomer complexes, quantum dots, dendrimers, and inorganic NPs including bismuth, gold, silica, and superparamagnetic iron oxide nanoparticles (SPIONs) [8,9].

## 1.2 Superparamagnetic magnetite nanoparticles ($Fe_3O_4$ NPs)

Magnetite ($Fe_3O_4$) NPs are inorganic materials with sizes ranging between 1 and 100 nm. Due to their small sizes, which allow them to have a high magnetic susceptibility and a single magnetic domain, $Fe_3O_4$ NPs (ferromagnetic materials with a grain size of less than 20 nm) exhibit superparamagnetic behavior (the ability to have zero magnetism in the absence of external magnetic field). $Fe_3O_4$ NPs have risen to prominence in many applications that facilitate the rapid advancement of nanoscale-based high-technology. $Fe_3O_4$ NPs have exhibited exceptional features, including ease of synthesis, small sizes, relative non-toxicity, slow oxidation, superparamagnetic crystal, and strong magnetic properties [10,11], and their potential as a promising

candidate for a wide range of biomedical applications, such as targeted drug delivery, biosensors, tumor detection and treatment, magnetic hyperthermia, and magnetic resonance imaging (MRI) has been validated [12–15].

### 1.3 Bismuth-iron oxide composite nanoparticles ($Fe_3O_4$@Bi NPs)

Despite extensive research on the exploration of $Fe_3O_4$ NPs, poor optical properties, and weak electrical conductivity hinders their widespread implementation [16]. Recent advances in $Fe_3O_4$ NPs research include not only the synthesis of homogeneous and stable core magnetic $Fe_3O_4$ NPs but also the formation of innovative nanostructures (functionalized surfaces, composites, core/shell, etc.) and the application of these nanomaterials in a variety of biomedical fields [17]. Composite NPs, particularly the core@shell structure that comprises distinct components, have recently been the subject of numerous investigations due to their unique physicochemical properties and multiple functionalities. The core@shell nanomaterials significantly improve intrinsic performance, overcome the restrictions of single-component properties, and exhibit a range of innovative features. Core@shell NPs typically composed of a core structure in the center and an exterior coated shell that varies in size, morphology, and organic/ inorganic interaction combinations. These NPs are capable of modifying the outer surface characteristics while retaining the properties of the inner core [18,19].

The application of $Fe_3O_4$ NPs can be expanded by incorporating new functional high atomic number (Z) groups into their structure, such as gold (Au) [20], silver (Ag) [21], and bismuth (Bi) [22]. Owing to their exceptional properties, which include high chemical stability, low toxicity, cost-effectiveness, high X-ray attenuation coefficient, strong absorbance of near-infrared (NIR) light, and high photo-to-thermal conversion

capability, Bi-based NPs have attracted considerable research interest for biomedical and *in vivo* applications [8]. Thus, Bi-incorporating $Fe_3O_4$ NPs are promising due to the combined advantages and properties of both components, enabling the development of $Fe_3O_4$ NPs applications such as double contrast agents for magnetic resonance imaging (MRI), and computed tomography (CT) scans, photothermal and magnetic hyperthermia therapies, and drug delivery.

## 1.4 Contrast agents (CAs)

Contrast agents are chemical compounds that enable the visualization of specific anatomical structures of the human body in medical imaging and are an essential component of many imaging techniques. Initially, contrasts were used to improve the visibility of vascular structures and the digestive (gastrointestinal) system. With the development of cross-sectional imaging techniques, contrast agents have become an integral part of medical imaging, allowing for better visualization and characterization of focal lesions in solid organs as well as better assessment of their vascularization and perfusion. Iodine- and barium-containing substances are extensively employed in X-ray-based imaging techniques (radiography, computed tomography (CT), fluoroscopy, and angiography), whereas gadolinium-containing chemicals are frequently used in magnetic resonance imaging (MRI). Depending on the targeted anatomical area, contrast compounds can be given intravenously, orally, or rectally [23].

NPs-based contrast agents can produce a much higher payload and much longer blood circulation half-life. The evolution of fabrication methods with multiple properties and different functionalities makes the NPs powerful that can be efficiently targeted in multimodality imaging or used as theranostic agents. Bi-containing NPs are very active and effective as ideal CT contrast agents and have more advantages over

currently used iodine (I)-based contrast agents and it is more appropriate for *in vivo* applications in comparison with other metals such as (Ag). Nevertheless, incorporating CT with other imaging probes is more suited for precise diagnosis by accumulating benefits and controlling defects of both imaging methods. Scientists are currently shifting from a single imaging modality (which usually cannot meet favorable diagnostic requirements) to a combination of different accurate imaging modalities. Therefore, combining CT with powerful MRI is convenient to acquire high-quality images and more accurate diagnosis [8,24–26].

### 1.5 Problem statement

Synthesis of bismuth-iron oxide composite NPs to allow control over their size, morphology, and surface coating is limitedly experienced. There are several methodologies have been employed to generate Bi/$Fe_3O_4$ composite NPs. However, the majority of them are limited and criticized by lengthy reaction time, long purification processes, and/or high reaction temperature [24,27,28], laborious synthesis process, complex growth mechanism, and high cost with utilizing multiple reagents [22,26,29,30]. Direct coating is an example of a technique that appears straightforward but is rather challenging due to the intricate steps of integrating two seemingly mismatched surfaces. In addition, the integration of Bi into the $Fe_3O_4$ core resulted in hybrid NPs with extremely low saturation magnetization and non-superparamagnetic properties [24]. Consequently, the incorporation of Bi into $Fe_3O_4$ must be technologically improved, particularly in minimizing hazardous reagents and controlling the particle size, magnetic characteristics, and composition of the NPs. Sonochemical (the application of high-intensity ultrasound) is a facile, rapid, non-conventional, and versatile approach that can be used to synthesize $Fe_3O_4$@Bi NPs.

Under physiological conditions, chemical stability and monodisperse are the main promising properties of nanocomposites for medical and related applications [31]. In addition, highly biocompatible and non-aggregated NPs are desired for biomedical applications. Uncoated $Fe_3O_4$@Bi NPs are unstable in aqueous solutions due to the strong affinity of $Bi^{3+}$ for hydroxide ions and susceptibility of $Fe_3O_4$ for surface oxidation, then the nanocomposites eventually promote precipitation, resulting in agglomeration of the nanostructures [8,32]. To address this issue, most of previous studies utilized chemical organic acids and polymers in the preparation of Bi/$Fe_3O_4$ composite NPs [8,33,34], which are costly synthetic reagents, resulting in inadequate stability [22,24,26], and some organic acids are toxic and make NPs biologically incompatible. Due to the presence of multiple biocompatible organic acids and amino acids in their structure, it may be advantageous to use *Sumac* extract solution as a stabilizing and capping agent in the fabrication process to produce stable, monodispersed, and biocompatible NPs [35–38].

It is critical to systematically design the experiment and scientifically optimize the fabrication process for the composite NPs to obtain the optimum result with a limited or minimum number of experiments. However, few reports highlighted the optimization of nanocomposites and the protocol for optimizing the stability and hydrodynamic size of $Fe_3O_4$@Bi composite NPs has not been established. Hence, $Fe_3O_4$@Bi NPs need to be well dispersed and stabilized, and their hydrodynamic size must be optimized in an aqueous media. Response surface methodology (RSM) is a powerful mathematical and multivariate statistical technique that can be used to develop and optimize $Fe_3O_4$@Bi NPs [16,39–41].

Nanocomposites-based dual CT/ MRI contrast agents must greatly induce X-ray attenuation and have high-efficiency $T_2$-weighted MRI contrast. Dedicated efforts have

presented the synthesis of Bi/$Fe_3O_4$-based contrast agents comprising assembly composition and core@shell structure. In a previous study, hybrid Bi/$Fe_3O_4$ NPs indicated good CT contrast due to the high bismuth proportion, but with extremely low transverse relaxivity which exhibited poor magnetic properties [24]. In contrast with another study, the Bi/$Fe_3O_4$ core@shell structure provided an effective $T_2$-MRI contrast agent due to its superparamagnetic behavior, along with attenuated X-ray only at high concentrations [29]. Nonetheless, none of these studies elucidated the foremost reasons for the inadequacy of $Fe_3O_4$@Bi in their compositions as dual-modal contrast agents. The core@shell structures have recently accumulated substantial interest compared to the combined assembly nanocomposites [28,29,42]. Sonochemical is recently shown as a prominent process to affect the structure and modifies the surface of $Fe_3O_4$ NPs. Although nanostructure experiments have proven the impact of sonochemistry on the deposition of organic and inorganic materials on the surface of $Fe_3O_4$ NPs [42,43], the evaluation of the synthesis of biocompatible $Fe_3O_4$@Bi composite NPs in a core@shell nanostructure through sonochemical method has not been examined and the effect of ultrasonication on the deposition of Bi on the surface of $Fe_3O_4$ NPs remain unexplored.

In this study, a simple and rapid sonochemical method was investigated to synthesize $Fe_3O_4$@Bi composite NPs with distinctive physiochemical properties, including high stability, monodispersity, uniformity, and high biocompatibility, along with the potential application as a dual-modal contrast agent for MRI and CT imaging. This research also aimed to optimize the sonochemical conditions for the efficient coating of Bi shell on $Fe_3O_4$ core NPs to produce biocompatible and exceptionally stable $Fe_3O_4$@Bi NPs. Using a statistical experimental design that was controlled by FCCD in RSM, several detectable parameters, including bismuth precursor, sodium

borohydride, and sonication time were employed to optimize the zeta potential value, hydrodynamic size, polydispersity indexes of the as-synthesized $Fe_3O_4$@Bi NPs.

## 1.6 Objectives of the study

The main aim of this study is to accomplish fundamental research on the implementation of a new technique for synthesizing extremely stable, highly magnetic, and biocompatible core@shell $Fe_3O_4$@Bi composite NPs that have the potential to be highly sensitive as a dual-modal contrast agent for MRI and CT applications. Compared to the conventional methods, this new technique of ultrasonically incorporating $Fe_3O_4$ with Bi NPs is straightforward, rapid, and inexpensive requiring few reagents. Several specific objectives of this study are summarized in the following points:

1. To rapidly synthesize highly stable biocompatible $Fe_3O_4$@Bi composite NPs via the sonochemical method.
2. To optimize the synthesized $Fe_3O_4$@Bi nanocomposites using FCCD in RSM, and examine the interaction effects between the independent variables (factors) on the dependent variables (responses).
3. To characterize the physicochemical properties of the optimized $Fe_3O_4$ and $Fe_3O_4$@Bi NPs.
4. To assess the cytotoxicity and cellular uptake (internalization) of the $Fe_3O_4$@Bi composite NPs by THLE-2 and HEK-293 cells.
5. To evaluate the sensitivity of the $Fe_3O_4$@Bi nanocomposites synthesized under optimal synthetic conditions as a dual-modal contrast agent for MRI and CT imaging.

## 1.7 Scope of the study

This study focuses solely on the synthesis of $Fe_3O_4$ core coated with Bi shell to rapidly produce extremely stable, biocompatible $Fe_3O_4$@Bi composite NPs using a sonochemical approach. In response surface methodology (RSM), a face-centered central composite design (FCCD) was used exclusively for the optimization procedure. The tip size horn, frequency, amplitude, and power of the ultrasonic probe are limited to 1.3 cm, 20 kHz, 40%, and 750 Watts, respectively. The agar phantoms containing different concentrations of $Fe_3O_4$@Bi NPs were employed as dual-modal contrast agents in both MRI and CT scans.

## 1.8 Thesis outline

This thesis is divided into six chapters. Chapter 1 contains the introduction, problem statement, aims, and objectives of this thesis. Chapter 2 presents a review of the literature on the synthesis of $Fe_3O_4$ NPs, $Fe_3O_4$@Bi composite NPs, and surface modification with various organic and inorganic materials, as well as their cytotoxicity and biocompatibility. Chapter 3 discusses the various theories that were used to support this research. The entire experimental procedure, characterization techniques, and application of the as-synthesized $Fe_3O_4$@Bi nanocomposites as a double contrast agent for CT and MR imaging are described in Chapter 4. The details of the various results observed in this work are highlighted and discussed in Chapter 5. In Chapter 6, the conclusion and future work of this thesis are presented.

# CHAPTER 2

# THEORY

## 2.1 Introduction

This chapter describes the fundamentals of sonochemistry, focuses on the effect of the acoustic cavitation process in liquids, and provides details on the physical, chemical, and thermal influences of the cavitation phenomena. In addition, the effects of ultrasound on the stability of NPs are also discussed in this chapter. Furthermore, the design of experiments (DOE) and central composite design (CCD) techniques for optimizing the response(s) of a system are also explained. Finally, this chapter discusses the theories, principles, mechanisms, and applications of MRI and CT-Scan, as well as dual CT/MRI contrast agents.

## 2.2 Theory of sonochemistry

The application of intense ultrasound on molecules to initiate chemical reactions and processes in liquids is called “sonochemistry”. The chemical effects of ultrasound do not result from a direct interaction between the ultrasound and chemical species at the molecular level. They originate from nonlinear acoustic events, specifically acoustic cavitation. Ultrasound is a component of the acoustic spectrum ranging from around 20 kHz to 10 MHz and is categorized into three major regions based on its frequency ranges, as depicted in Figure 2.1: (1) low frequency with high power ultrasonic waves (20 kHz to 100 kHz), (2) high frequency with medium power ultrasound (100 kHz to 1 MHz), and (3) high frequency with low power ultrasonic waves (1 MHz to 10 MHz).

However, ultrasonic frequencies ranging from 20 kHz to about 1 MHz are used in the field of sonochemistry, whereas frequencies significantly higher than 1 MHz are utilized in the field of sonography, which is a medical and diagnostic application of

ultrasound [44,45]. By exposing water or liquids to ultrasonic irradiation, high and low-pressure regions are created within the liquid due to the periodic expansion and compression of the ultrasonic waves. This uniqueness in liquids initiates the acoustic cavitation phenomenon, which consists of bubble formation, expansion, and collapse [46]. The energy absorption from rarefaction and compression grows the ultrasound-produced bubbles. After a few sonic cycles, the bubbles will reach a threshold size and collapse rapidly. During the fast-transient collapse of the bubbles, it is assumed that almost no heat is transferred from the interior to the surrounding media. Consequently, the pressure and temperature that are built up inside the sphere of the bubbles rise to around 1000 atm and 5000 K, respectively [47]. The region of the core that has the maximum pressure and temperature is known as the “hot spot”. After the bubbles have collapsed, there is a rapid transfer of heat from the high-temperature region of the collapsed bubbles to the surrounding liquid at a rate of around $10^{10}$ K/s. In addition, the pressure difference between the inner and outer regions of the bubbles produces a “shock wave”. This shock wave and radicals created by the thermal breakdown within or close to the bubbles play an important role in the cavitation phenomena that takes place in sonochemistry. Sonochemistry is affected by the ultrasound's operational parameters, including input power, ultrasound frequency, ultrasonic intensity, dissolved gases, and bulk temperature [48].

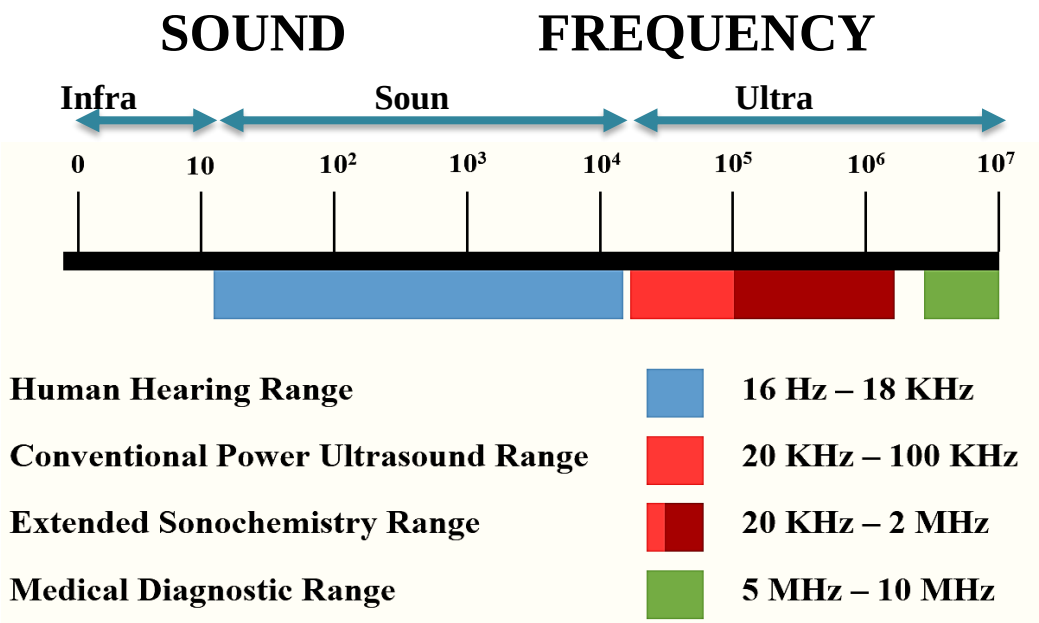


Figure 2.1 Classification of sound based on its frequency ranges.

### 2.2.1 Acoustic cavitation and bubble formation

The process of acoustic cavitation is considered to be the basis of sonochemistry. The term "cavitation" refers to the formation of tiny compressed gas bubbles (cavities) inside of a homogeneous liquid medium. It is a physical phenomenon that can result from an abrupt decrease in pressure [49]. As shown in Figure 3.2, the cavitation phenomenon is created when ultrasonic waves propagate through a liquid and induce pressure variations [50]. Irradiating a liquid with ultrasonic waves causes the molecules in the liquid to move in an oscillatory pattern, and this pattern is then transmitted through the liquid by pressure waves. Consequently, it creates rarefaction and compression waves in the molecular structure of the liquid. This results in the liquid molecules vibrating around their position. As the ultrasonic intensity within the liquid is increased, the distances between the molecules can also increase and the intramolecular tensions within the molecular structures can be dissipated. The molecules of the liquid break down and a cavity known as a cavitation bubble is created. These bubbles expand and compress in response to the ultrasonic field within the liquid,

and then eventually collapse. This process, which includes bubble formation, expansion, and collapse, is known as “Acoustic Cavitation” [50–52].

Acoustic cavitation is the formation and collapse of pre-existing microbubbles in liquids under the ultrasonic field. The cavitation bubbles can be characterized by the dynamics of their distinctive oscillations and the highest temperatures and huge pressures obtained when they explode. The level of cavitation depends on the transducer; different transducers produce different levels of cavitation. When it comes to horn-type transducers, the sound energy is focused at the tip of the horn (usually between 20 and 100 kHz). This causes the development of discrete cavitation and high movement of fluids in the area near the tip of the horn [53]. Plate-type transducers, which operate between 20 kHz and 2 MHz and have a diameter of about 5.0 cm, allow for greater sound-wave dispersion and, hence, greater wave propagation over the entire liquid. Thus, horn transducers are used for low liquid volumes and high energy concentration in a short region, while plate transducers are used for larger volumes and more uniform wave fields.

The cavitation bubble can be categorized as either stable or transient. In stable cavitation, a bubble can undergo multiple vibrational cycles of refraction and compression before collapsing, whereas in transient cavitation, bubbles expand double their size in one sonic cycle and then collapse [54]. The number of bubbles that are present at the active site, the size of the active bubbles, and the intensity of bubbles collapse are all influenced by the geometry of the reactor vessel, liquid height, and the type of solution, as well as the power, frequency, and solution conditions of the sonication process [55]. High-frequency cavitation bubbles tend to be stable, but the transient cavitation bubbles that result from low frequency are frequently unstable. The overall implication is that the size of active bubbles decreases with increasing

frequency, therefore the collapse intensity would be proportionally smaller at higher frequencies. However, due to increasing antinodes in the solution, the increasing frequency rises the number of active bubbles [56–58]. These factors make sonochemistry difficult to compare their investigations from different systems and different research groups. The implosive collapse of bubbles is frequently producing hot spots with temperatures of about 5000 K, pressures of 1000 atm, and cooling rates of $10^{10}$ $Ks^{-1}$ (Figure 2.2). Nevertheless, transient cavitation is more powerful than stable cavitation.

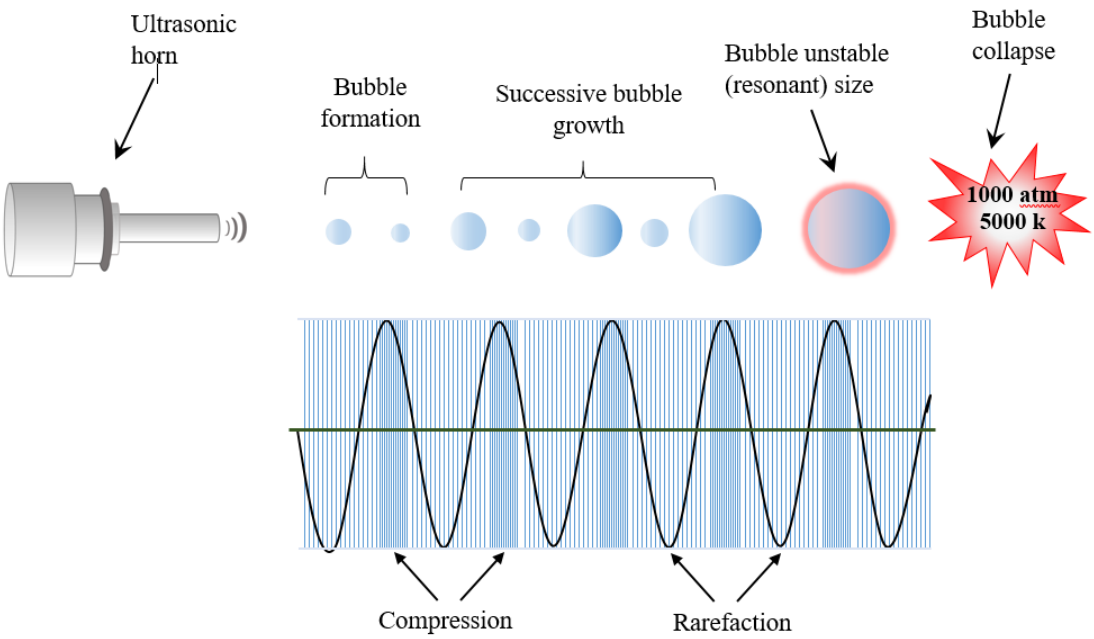


Figure 2.2 Schematic representation of the acoustic cavitation process.

### 2.2.2 Effect of acoustic cavitation

The frequency that is most commonly employed in sonochemistry is a low ultrasonic frequency ranging from 20 KHz to 40 KHz. This frequency does not have a direct influence on any of the physical, chemical, or biological effects. Since the frequency is so low, there is no possibility of a direct interaction between the ultrasound and the substance (chemical species). Nevertheless, the acoustic cavitation process of the ultrasound and materials can interact indirectly. The concentrated energy created

from the collapsed microbubbles is sufficient to affect molecules. Compared to other conventional energy sources, ultrasonic irradiation provides several unique and exceptional reaction conditions by the acoustic cavitation process (a short duration of extremely high temperatures and huge pressures in liquids) which cannot be procured from other techniques [44]. These conditions can result in a wide array of physical, mechanical, chemical, and biological effects, enabling the application of the acoustic cavitation process in several fields, including food extractions, drug transport, medical imaging, water treatment, emulsification, cleaning surface of materials, sonocatalysis, sonoluminescence, and sonochemistry [55].

#### 2.2.2(a) Physical effects

A number of different physical phenomena, such as microjets and shock waves, often appear alongside the localized hotspot after the sonic bubble collapses [59]. The creation of these physical phenomena relies mainly on the discrete features of the medium, which may be a homogeneous (uniform liquid) or a heterogeneous (non-uniform) medium. In the homogeneous liquid, acoustic cavitation generates symmetrical cavitation as well as shock waves with high pressures greater than 1 kbar. However, in a non-homogeneous medium (solid-liquid interface), asymmetric cavitation and high-speed microjets are generated, which disrupts the solid surface and leads to mechanical damage [60,61]. Benjamin and Ellis (1966) and Naude and Ellis (1961) were the first to observe microjets experimentally. The greater velocity of the microjet (usually more than 100 m/s) suggests a conversion of the collapsing bubble's potential energy into kinetic energy [62]. In contrast, the formation of microjets during the acoustic cavitation process at the solid-liquid interface depends highly on the size of the interface [63]. The size of the collapsing bubbles must be greater than the solid barrier. If the ultrasonic field has a frequency of 20 kHz and the solid particles are

smaller than the diameter of the collapsing bubble (less than 150 μm), then the ultrasonic field is incapable of initiating the formation of microjets since the environment is homogeneous; as a result, regular cavitation and the emission of shock waves will take place. In contrast to microjets, which produce mechanical damage to materials such as erosion and pitting, shock waves create a powerful force that causes random acceleration of the NPs at considerable velocities, leading to inter-particle collisions [64,65].

#### 2.2.2(b) Chemical effects

The chemical reaction generated by ultrasonic irradiation can be attributed to a localized hotspot and extraordinary conditions caused by the collapsing of bubbles [55]. The hotspot is an appropriate way for concentrating the diffused (dispersed) sound energy. The chemical effects of ultrasonic waves have been described by Richards and Loomis for the first time in 1927. Several researchers have deployed this unique effect of ultrasonic acoustic cavitation to easily and rapidly fabricate a wide range of nanostructures [65].

## 2.3 Effect of ultrasound on the stability of NPs

The particles of a colloidal system are considered stable if they can remain in an equilibrium state while suspended in a solution. The stability of a colloidal system is determined by the uniform distribution of colloidal particles in the layers of the solution. More particles suspended in layers increase the stability of the colloidal system. The zeta potential is a measure that can be utilized to determine the stability of a colloidal solution. Experimental studies indicate that the use of ultrasonic treatment breaks down large clusters of NPs into smaller clusters or even individual NPs. Figure 2.3 graphically depicts the sonochemistry treatment mechanism. In sonochemistry, the acoustic

cavitation process also aids to preserve the stability of nano-fluids and colloidal solutions by functionalizing the surface and structure of the NPs, hence preventing clusters from agglomerating [66,67]. The use of sonochemistry has made it possible to study the dispersion behaviors of numerous nano-fluids. Therefore, it is essential to analyze the particular sonochemistry conditions for various nano-fluids. Related researches also suggest that direct sonochemistry (the use of a probe/horn) is more effective than the use of indirect sonochemistry (bath sonicator) for dispersing NPs in a base liquid/solution [68]. Therefore, to get the optimal dispersion, researchers must conduct benchmark studies on the efficiency of sonochemistry parameters, such as power, frequency, time, type of sonochemistry (probe or bath), probe diameter, etc., for various types of NPs, such as metals and metal oxides. Moreover, the best sonochemical conditions for a nanofluid are characterized by the smallest increase in viscosity and the largest increase in heat conductivity [49].

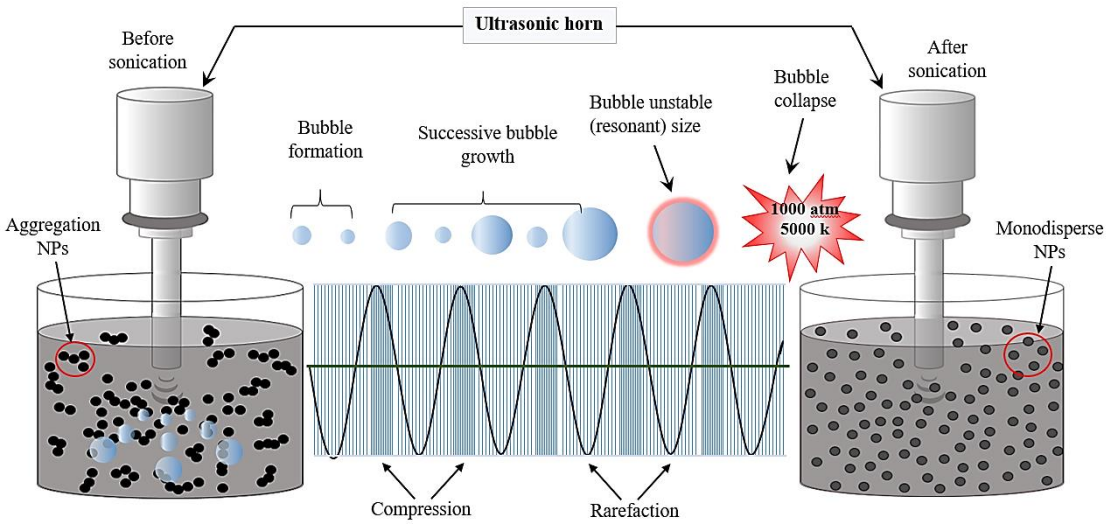


Figure 2.3 Schematic illustration of braking down the NPs' agglomeration by sonochemistry.

## 2.4 Properties of $Fe_3O_4$ NPs

Magnetite, maghemite, and hematite are the most common forms of IONPs. Among them, hematite is the most chemically stable phase in the presence of air over

an extended duration of time. However, hematite possesses the lowest magnetic strength [69,70]. The word "magnetite" originates from the region of Asia Minor known as "Magnesia," which is the location where significant deposits (quantities) of the mineral were found. Due to its presence of both ferric (oxidized) and ferrous (reduced) iron atoms, magnetite is frequently inferred to be iron (III) oxide [71,72]. The following chemical composition depicts a typical magnetite production reaction:

$$FeO \text{ (Ferrous oxide)} + Fe_2O_3 \text{ (Ferric oxide)} \rightarrow Fe_3O_4 \text{ (magnetite)}$$

### 2.4.1 Structural and physical properties

Iron oxide is a typical chemical compound comprised of iron and oxygen atoms. The chemical formula and composition of magnetite are, respectively, $Fe_3O_4$ and $Fe^{2+}(Fe^{3+})_2(O^{2-})_4$. Magnetite possesses a crystalline structure, which is a face-centered cubic lattice and inverse spinel structure, and comprises octahedral and mixed tetrahedral/octahedral layers packed along the (111) plane, wherein $O^{2-}$ ions form a cubic structure while $Fe^{2+}$ and $Fe^{3+}$ occupy interstitial sites (1/3 tetrahedral and 2/3 octahedral), as displayed in Figure 2.4 [70–72]. Unlike other forms of iron oxides, $Fe_3O_4$ is unique because it includes both divalent ($Fe^{2+}$) and trivalent ($Fe^{3+}$) iron ions. Physically, the colloidal suspension solution and powder form of pure magnetite can be identified by the shiny jet-black color. However, bare $Fe_3O_4$ oxidizes to $\gamma$-$Fe_2O_3$ when it is exposed to air (oxidation), which is characterized by its brownish color [70].

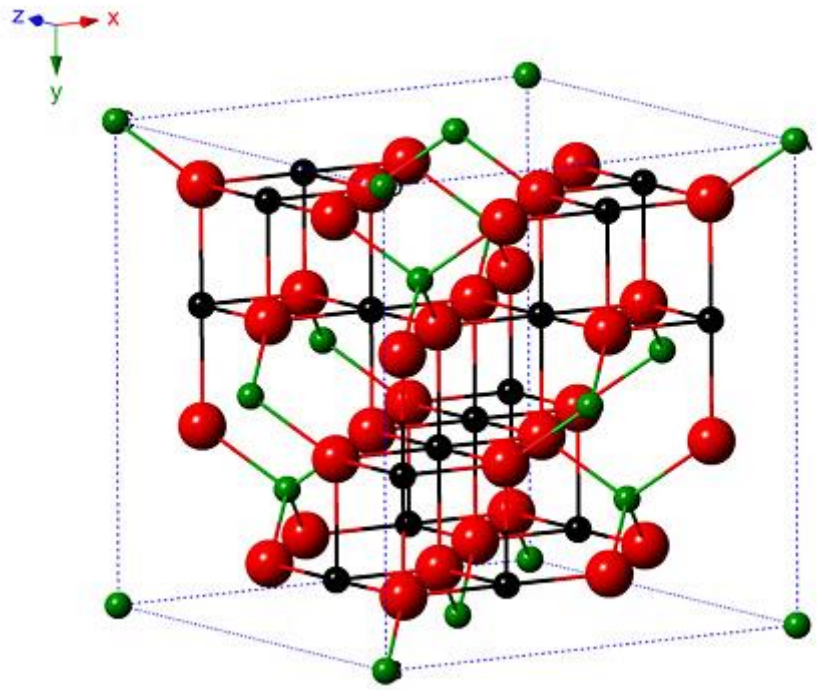


Figure 2.4 The Crystal structure of $Fe_3O_4$. The green balls denote the ($Fe^{3+}$); the black balls denote the ($Fe^{2+}$), and the red balls denote the ($O^{2-}$) [71].

### 2.4.2 Magnetic properties

Iron oxides possess an intrinsic magnetic property. Nevertheless, the magnetic strengths of iron oxides are varying. The magnetic dipole moments of a magnetic material (a tendency measure of a material to align with a magnetic field) are originated from the spin and orbital motion of the electron, as well as the interactions between electrons. The 3d electronic orbital is crucial for regulating the unique properties of the iron (Fe) atom. Due to the presence of four unpaired electrons in the 3d orbital, iron atoms often possess a significant magnetic moment. $Fe^{2+}$ and $Fe^{3+}$ ions have $3d^6$ (four unpaired electrons) and $3d^5$ (five unpaired electrons), respectively. $Fe^{+2}$ and $Fe^{3+}$ ions undergo magnetically ordered phase changes below the transition temperature and become ferromagnetic, antiferromagnetic, or superparamagnetic [72–74].

As shown in Figure 2.5, the magnetism of materials can be categorized as diamagnetic, paramagnetic, or ferromagnetic based on their response and orientation to an externally applied magnetic field. In addition to ferromagnetic, there are also

ferrimagnetic and antiferromagnetic materials [75]. Diamagnetism is a distinguishing property of a material that exists only in the presence of an external magnetic field. However, the net magnetization value is zero in the absence of this magnetic field. When a magnetic field is applied, magnetic dipoles point in the opposite direction of the applied magnetic field. Therefore, a diamagnetic material has a negative and lower magnetic susceptibility ($-10^{-6}$) [76].

Paramagnetic materials have unpaired electrons and a small positive susceptibility to an external magnetic field. These materials have a weak magnetic attraction to the magnetic field, the dipole moments are randomly aligned, and lose their magnetism when the applied magnetic field is removed. In contrast, when the magnetic field is applied, all magnetic dipoles become uniformly aligned in the same direction of the magnetic field.

Unlike paramagnetic, ferromagnetic materials possess a large positive susceptibility to an external applied magnetic field. Ferromagnetic materials are strongly attracted to the applied magnetic field and retain their magnetic characteristics after the field is removed. Ferromagnetic materials also include unpaired electrons; therefore, their atoms possess a permanent net magnetic moment (magnetization). This permanent magnetic moment in a ferromagnetic material is due to the un-canceled electron spins in its electron structure. All magnetic moments align in the direction of an applied external magnetic field until saturation magnetization (*Ms*) is attained. When the magnetic field is removed, the magnetization does not instantly return to its initial value. Instead, there is a remanent magnetization (*Mr*) and a coercivity field (*Hc*) which is required to return the system to its initial state. However, antiferromagnetic materials have zero net magnetization because the external magnetic field causes magnetic moments to align antiparallel [17,32].

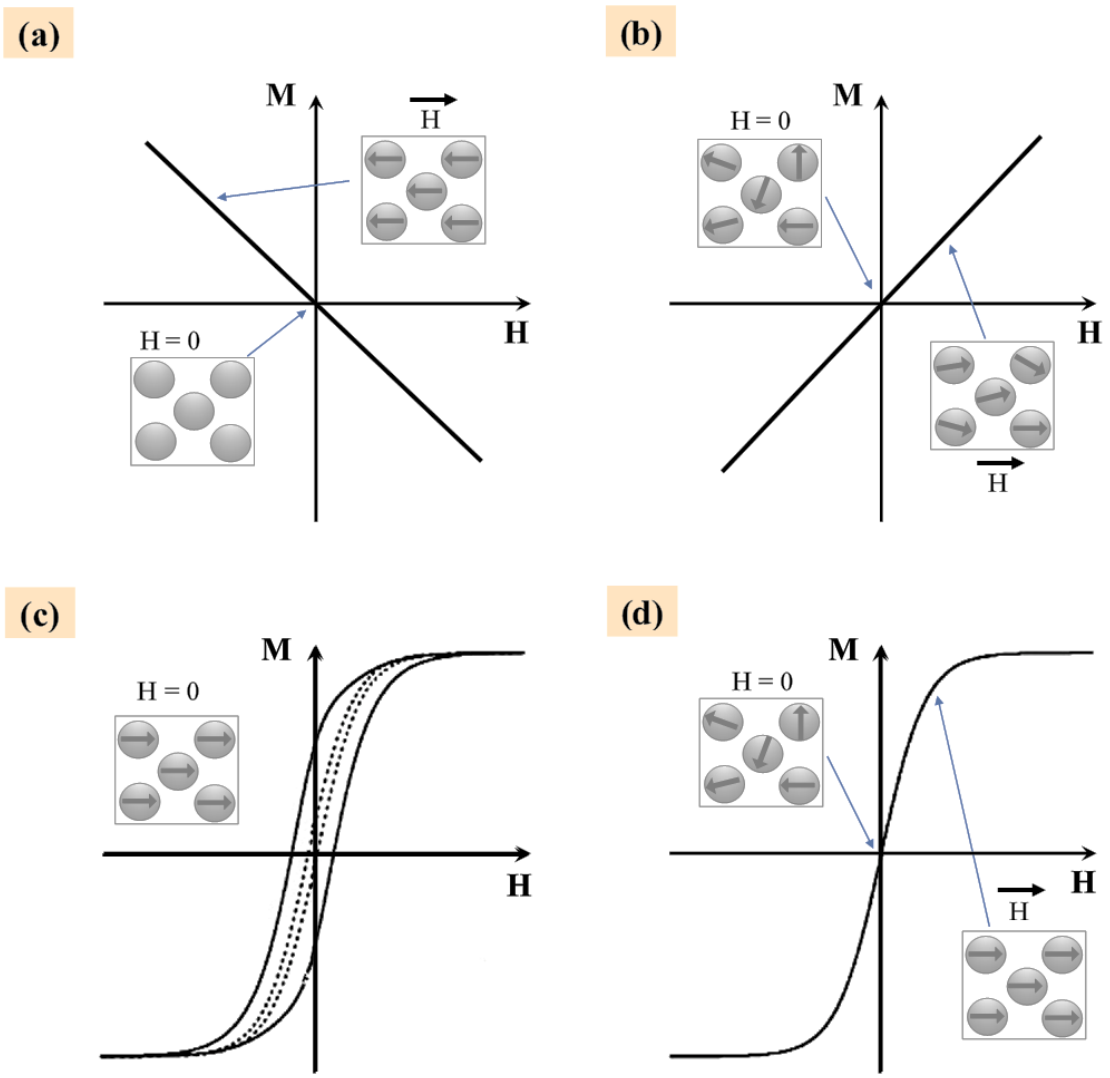


Figure 2.5 M-H curves, a schematic illustration of magnetization as a function of an applied magnetic field (a) Diamagnetic material, where magnetic moment (M) decreases as the external magnetic field increases (H). (b) For paramagnetic material, M increases with H. (c) Ferromagnetic material demonstrates a hysteresis loop with remanence (Mr) and coercivity (Mc). (d) Superparamagnetic material that has a similar sigmoid shape to ferromagnetic material with no hysteresis loop, remanence, and coercivity.

Nevertheless, ferromagnetic and ferrimagnetic NPs exhibit superparamagnetic behavior, a property in which magnetic materials strongly respond (have a substantially higher magnetic susceptibility than typical paramagnetic materials) and their magnetic moments rapidly align to the same direction (parallel) of an externally applied magnetic field without magnetic memory, no *Hc* and no *Mr*. In other words, superparamagnetic materials do not maintain any net magnetization when the external magnetic field is

removed. Superparamagnetic materials have magnetic anisotropy, which generally refers to the preferred alignment of their magnetization. Bulk iron oxides, particularly $Fe_3O_4$ with average particle diameters up to 100 nm, have a multi-magnetic domain structure. When the size of the NPs is reduced to less than 30 nm, a single domain (a region in which the magnetic fields of atoms are aligned) eventually will be formed, and thus $Fe_3O_4$ NPs become superparamagnetic [77,78].

## 2.5 Properties of Bi NPs

Due to their distinctive optical and electrical properties, inorganic particles, particularly metal NPs, have been extensively researched and developed in various fields. As a semimetal with a relatively narrow band gap, bismuth (Bi) is an essential component in a variety of existing technological applications. In place of Bi bulk materials, Bi-based nanoscale particles have recently attracted considerable scientific interest for advanced technological applications. Bi NPs exhibit unique features that are absent or substantially different from their bulk materials [79]. Recent investigations for the formation of nanosized Bi-containing materials have shifted from chemical, electrical, optical, and engineering to biomedicine due to their biosafety, low-cost production techniques, and tunability in size, shape, and porosity. Bi has been exploited to synthesize diverse NPs with distinct physicochemical, structural, and compositional characteristics to combine a variety of properties [80].

Among plenty of investigated inorganic and organic nanostructures for potential biomedical applications, single elemental Bi NPs and Bi-based NPs have recently attracted much research attention due to their incredible chemical, physical, and biological properties which include excellent chemical stability, relative non-toxicity, high surface area, cost-effectiveness, simplicity of functionalization, high electrical,

diamagnetic and magnetoresistance properties under the influence of a magnetic field, suitable catalytic activity, chemical inertness, radiostability, radiosensitization, high X-ray attenuation coefficient, and photo-to-thermal conversion efficiency, favorable near-infrared (NIR) absorption, and lengthy blood circulation half-life. Additionally, compared to other heavy metals like silver, Bi is thought to be one of the most biocompatible and low-toxic materials for *in vitro* and *in vivo* applications [8,81].

Nanomaterials with high atomic numbers (Z) have a high attenuation coefficient, demonstrating their utility as contrast agents for computed tomography (CT) imaging. Bismuth has various biomedical advantages over other high Z elements. Due to its highest atomic number (Z = 83) among non-radioactive substances, Bi has a larger X-ray attenuation coefficient (5.74 $cm^2/g$ at 100 keV), resulting in its higher CT contrast agent. In addition, elemental metal Bi strongly absorbs light throughout a wide spectral range that extends into the infrared (IR), enabling the photothermal heating of elemental Bi NPs by an IR light to be employed for photoacoustic imaging as well as photothermal therapy, which can synergistically enhance radiotherapy [82,83]. Furthermore, due to its good chemical reactivity, dissolving capabilities, and bioactivity, Bi can easily be excreted from the body. These distinctive properties make Bi NPs more appealing for biological applications than other metal-based NPs.

Bi has conventionally been deployed in the fabrication of pharmaceuticals for the treatment of many diseases such as hypertension, gastrointestinal, and syphilis; however, in recent years, the application of Bi-based nanoscales has developed dramatically in diverse biomedical fields, such as bio-imaging, combined cancer therapy, X-ray radiotherapy, biosensors, heavy metal ion detectors, tissue engineering, and antimicrobial formulations has expanded dramatically [73,76]. Bulk Bi is a semimetal with long Fermi wavelengths, strong diamagnetism, and high

magnetoresistance, that may be utilized to create various forms and compositions of BiNPs. Besides, Bi single-component NPs (elemental BiNPs) can be employed as intermediates in the fabrication of additional types of BiNPs [73,84–86]. Bi-chalcogenides, which belong to group VI of Bi compounds, Bi-oxyhalides, and other forms of Bi nanostructures are among the most interesting types of Bi-based NPs with adopting various structures and morphologies as illustrated by a diagram in Figure 2.6. In addition to their chemical stability, the nanoscale structures of these Bi-compounds exhibit inherent electrical and optical properties, making them particularly suitable for a variety of biomedical applications [8,80,81]. Similar to the synthesis of iron oxide NPs, Bi-containing NPs have been fabricated using different physical, chemical, and biological methodologies, including laser-mediated approaches, chemical reduction methods, hydrothermal/solvothermal synthesis, sol–gel approaches, microemulsion techniques, evaporation routes, microwave irradiation, and sonochemical synthesis [8].

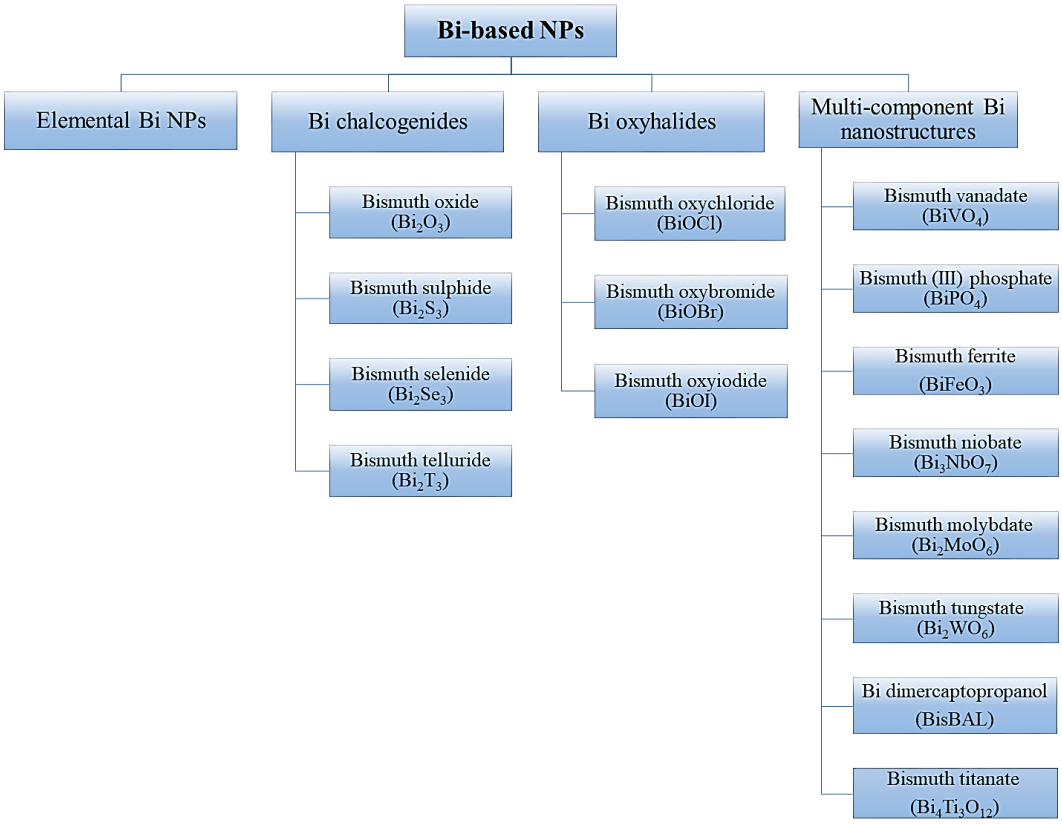


Figure 2.6 Schematic diagram of the most common types of Bi-based NPs.